Numerical investigation of subgrid mixing effects on the calculation of biological reaction rates

Marion Linkes, Pascal Fede, Jérôme Morchain, Philippe Schmitz

Numerical investigation of subgrid mixing effects on the calculation of biological reaction rates

Marion Linkès [a,b], Pascal Fede [a,b], Jérôme Morchain [c,b,*], Philippe Schmitz [c,b]

[a] Université de Toulouse, INP/UPS/IMFT, allée du Professeur Camille Soula, 31400 Toulouse, France
[b] CNRS, Fédération FERMAT, 31400 Toulouse, France
[c] Université de Toulouse, Laboratoire d'Ingénierie des Systèmes Biologiques et des Procédés, INSA/CNRS/INRA, 135 avenue de Rangueil, 31077 Toulouse Cedex, France

- DNS coupled with Lagrangian Particle Tracking in a HIT box are performed.
- Statistically steady concentration fluctuations are forced by a mean gradient.
- Substrate uptake rate distributions are deduced using a Monod model.
- The metabolic reaction rates at equilibrium are set by the average concentration.
- Reduced growth rate and overflow metabolism are related to imperfect micro-mixing.

Keywords:
Bioreactors
Mixing
Metabolic model
Direct numerical simulation
Statistical approach

A B S T R A C T

The consequences of substrate concentration heterogeneities at the cell level, on the behavior of microbial populations have been identified some years ago. However, subgrid effects are rarely considered in bioreactor modelling. In this paper, this central issue is investigated with Direct Numerical Simulations (DNS) coupled with Lagrangian particle tracking and scalar field calculations in the case of statistically steady homogeneous and isotropic turbulence. From these calculations, the exact distribution of substrate uptake rates of a microorganism population is calculated and compared, favorably, to analytical solutions. A metabolic model considering anabolism, oxidative catabolism and dissimilation is invoked to quantify the consequences in terms of overall reaction rates at the population scale. It is shown that imperfect mixing reduces the growth rate and increases the by-product formation while leaving the total uptake rate unchanged. This work provides a rational explanation, based on physical consideration, for the loss in biomass productivity and the increase of by-product formation in imperfectly mixed bioreactors.

1. Introduction

The existence of macromixing issues in industrial fermentors has been identified for years (Hansford, 1966; Bylund et al., 1998; Oosterhuis and Kossen, 1984; Enfors et al., 2001). These are related to the competition between momentum transfer, gas–liquid mass transfer and biological reaction at the reactor scale. The consequences are the formation of concentration gradients at the reactor scale and the cell exposure to concentration fluctuations. Numerous experimental works have also been devoted to the consequences of small scale mixing problems in lab-scale bioreactors (Amanullah et al., 2001; Hewitt et al., 2000; Dunlop and Ye, 1990). They revealed that cell populations are sensitive to the mixing rate in a well macromixed bioreactor (Garcia et al., 2009). Following the classification method proposed by Bourne (2003) these experiments refer to mesomixing. For many years identifying the effects of possible mixing issues in bioreactors has been extremely tedious for many practical reasons. The concentration field experienced by the cells was, from an experimental point of view, out-of-reach since the biological information was obtained at the population scale. Owing to recent microbiological techniques (such as flow cytometry) it is now possible to collect biological data at the cell scale and to use the cell as a reporter

* Corresponding author at: Université de Toulouse, Laboratoire d'Ingénierie des Systèmes Biologiques et des Procédés, INSA/CNRS/INRA, 135 avenue de Rangueil, 31077 Toulouse Cedex, France. Tel.: +33 561559774; fax: +33 561559400.
E-mail address: jerome.morchain@insa-toulouse.fr (J. Morchain).

that records and reveals the local environment encountered by the cell (Delvigne et al., 2009). Yet it is not easy to distinguish between the natural heterogeneity and that induced by a heterogeneous environment. The fact that the biological population state actually depends on the history of the cultivation is also a complicating factor. In particular, one key point in biological process is the mass transfer from the liquid to the biological phase, called assimilation or uptake. From a biological point of view, assimilation has been studied by Koch and Wang (1982), Ferenci (1996), Natarajan and Srienc (1999), Natarajan and Srienc (2000), Lin et al. (2001), Chassagnole et al. (2002), among others. One important conclusion concerns the ability of cells to modify their assimilation capacity in response to the concentration fluctuations they undergo. In practice, it is extremely difficult to draw out conclusions and to perform quantitative comparison between various biological experiments because the actual degree of mixing at the cell scale is generally not known. Anyway, the fact that a heterogeneous concentration field has an influence on the cell population is now clear (KaSZ et al., 2014). Garcia et al. (2009) showed that GFP (Green Fluorescent Protein) reporting strains sensitive to oxygen limitation were illuminated whilst cultivated in an agitated bioreactor with the DO (Dissolved Oxygen) maintained above 20% of the saturation concentration (far above the affinity constant for oxygen). It confirms that the mean concentration measured by a probe (macroscopically) may not reflect the actual concentration field experienced by the cells.

As an alternative to the experimental studies, numerical simulation has a certain number of potential advantages. In particular, Direct Numerical Simulation (DNS) allows the calculation of the instantaneous local velocity and scalar concentration field dynamics without making reference to a turbulence model. The Lagrangian tracking of particles results in the calculation of individual trajectories and histories which can be recorded (Lapin et al., 2004, 2006; Delafosse et al., 2009). Thus, the fate of each particle is known. Another major interest is to allow the calculation in well defined, steady and repeatable conditions. Although this technique is relatively popular in the fluid mechanics community (Boivin et al., 1998; Yeung, 1998; Taulbee et al., 1999; Reade and Collins, 2000) very little work has been done in the field of biochemical engineering. Coupled to the resolution of a concentration field, the Lagrangian tracking of particles was used to study the interaction between turbulence and chemotaxis (Taylor and Stocker, 2012).

The objective of the present work is to use this technique along with a simplified metabolic model to investigate the consequences of concentration heterogeneities below the resolved scale on the overall reaction rates exhibited by a population of cells. The resolved scale corresponds to the spatial resolution of the hydrodynamic model used to compute the velocity and concentration fields inside the bioreactor. The uptake rate distributions are computed numerically from the concentration distribution and the prescription of a substrate assimilation law. Numerical results are successfully validated against analytical solutions. A metabolic model is invoked for each specific uptake rate and a volume averaging is used to establish the overall reaction rates. This work can be regarded either as an attempt to explain what happens in a heterogeneous bioreactor or as a first step in the formulation of a closure model for the biological reaction. All calculations are performed considering that all cells are identical and that assimilation is controlled by an enzymatic reaction so that the uptake rate is modeled by a Michaelis–Menten law:

$$q_S = q_{S,\max}\frac{S}{k_S+S} \tag{1}$$

where $q_{S,\max}$ is the maximum specific uptake rate (in $\mathrm{mol_S\ g_X^{-1}\ h^{-1}}$), S is the substrate concentration at the cell position and k_S is the affinity for the substrate of an individual microorganism. It is different from an apparent affinity constant K_S which depends on macroscopic properties as explained in a previous paper (Linkès et al., 2012). The reduced variable $k_S/\langle S\rangle$ is used to perform parametric studies that cover the whole range of possible situations: from nutrient excess to severe limitation.

The first part of the paper is dedicated to a brief analysis of mixing and biological reaction times at various scales. Then a description of the DNS tool along with the calculation of the uptake rate distribution are proposed. The second part presents the main features of a simplified metabolic model including overflow metabolism as well as the analytical development leading to the calculation of the overall reaction rates. It will be shown that the overall substrate consumption rate is hardly affected by the degree of homogeneity whereas both the specific growth rate and the by-product formation are highly dependent on the actual substrate concentration distribution in the volume of fluid considered.

2. Mixing and reaction time scales in a bioreactor

2.1. Biological reaction time scales

In order to estimate the biological reaction time scales, we consider a simple unstructured kinetic model. The reaction rates for growth and uptake are given by the following equations:

$$r_X = \frac{dX}{dt} = \mu_{max}\frac{S}{K_S+S}X, \tag{2}$$

$$r_S = \frac{dS}{dt} = -q_{max}\frac{S}{K_S+S}X. \tag{3}$$

where $\mu_{\max}$ is the maximum specific growth rate and X is the cell concentration. For each reaction, a time scale, τ_C, can be defined as

$$\frac{dC}{dt} = \frac{C}{\tau_C} \tag{4}$$

which further leads to the following expressions of the bioreaction time scale for growth and substrate uptake respectively:

$$\tau_X = \frac{K_S+S}{\mu_{max}S}, \tag{5}$$

$$\tau_S = \frac{K_S+S}{\mu_{max}X} \approx \frac{S}{\mu_{max}X}. \tag{6}$$

It is clear from there that the two characteristic times obey different rules: the time scale for growth is independent of the cell density whereas the time scale for substrate consumption is inversely proportional to the cell density. The time scale for growth is only dependent on the strain considered. Most industrial strains grow at a specific rate between 0.1 and 1 $\mathrm{h^{-1}}$. The time scale associated (1–10 h) is systematically longer than all other characteristic times in a bioreactor (macromixing or gas–liquid mass transfer). Using this time scale to analyze mixing issues in bioreactor would lead to the conclusion that there can be no competition between mixing and biological reaction at any scale. This is in contradiction with many experimental observations reported above. In fact, the pertinent time scale when dealing with a competition between mixing and reaction in a bioreactor is the time scale related to substrate consumption. This characteristic time depends on the amount of cells that actually consume the substrate. It gets smaller as the number of cell increases, which clearly makes sense. Increasing the cell density pushes the biological reactor towards a more severe competition between mixing and substrate uptake. Considering typical value for the maximum specific uptake rate ($2\ \mathrm{g_{S}\ g_X^{-1}\ h^{-1}}$), a cell density

Table 1
Time (in seconds) and length scales of mixing in two bioreactors (lab-scale 3L, industrial scale 20 m^3) equipped with a Rushton turbine. Average power input $\epsilon_V = 1.3$ kW m^{-3} in both cases. t_C, macromixing time; t_S, mesomixing time; t_E, micromixing time due to engulfment; t_D, micromixing time due to diffusion; Λ, Taylor macro scale; η_k, Kolmogorov scale; η_B, Batchelor scale.

Mechanisms	Time scale	Length scale	Labscale	Industrial
Macromixing	$t_C = \frac{V}{1.8\ N_{Q_g}\ N\ D^3}$	$V^{\frac{1}{3}}$	0.8	13
Mesomixing	$t_S = 2\left(\frac{\Lambda^2}{\epsilon}\right)^{1/3}$	$\Lambda = w,\ \Lambda = \frac{1}{2}\frac{k^{3/2}}{\epsilon}$	0.03	0.2[a]/0.55[b]
Micromixing (engulfment)	$t_E = 17\left(\frac{\nu}{\epsilon}\right)^{1/2}$	$\eta_K = \left(\frac{\nu^3}{\epsilon}\right)^{1/4}$	0.015	0.015[a]/0.07[b]
Micromixing (diffusion)	$t_D = 2\left(\frac{\nu}{\epsilon}\right)^{1/2}\text{arcsinh}(0.05\ Sc)$	$\eta_B = \left(\frac{\nu\ D_m^2}{\epsilon}\right)^{1/4}$	0.008	0.008[a]/0.026[b]

[a] Based on the average energy dissipation rate.
[b] Based on a twentieth of the average energy dissipation rate (far from the impeller).

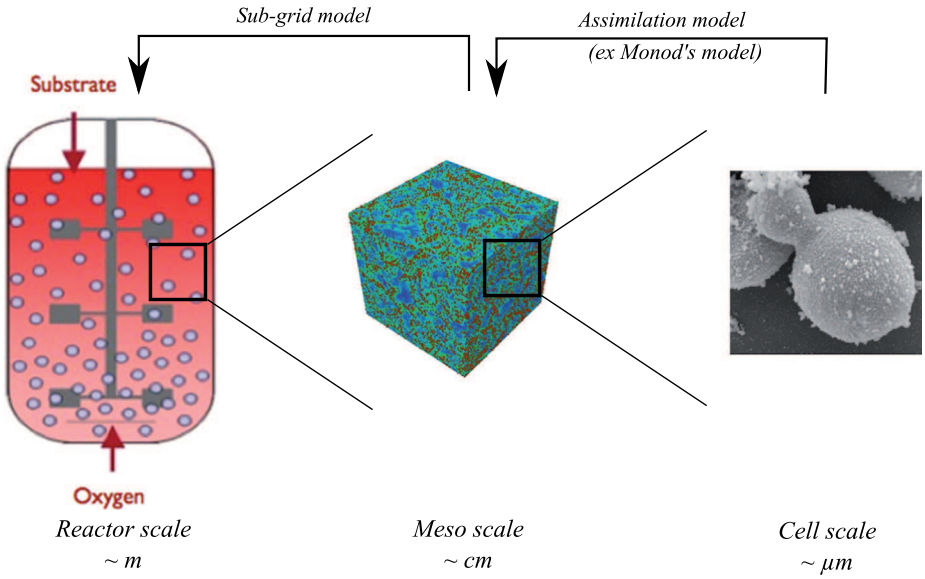

Fig. 1. Multiscale modelling methodology: integration of small scale concentration heterogeneities in the calculation of the biological reaction rates.

between 10 g L^{-1} and 50 g L^{-1} and a residual concentration between 10 mg L^{-1} and 50 mg L^{-1} leads to characteristic assimilation times ranging from 0.1 to 7.5 s. These values will further be used and compared with the mixing time at various scales.

2.2. Mixing time scales

The characteristic times scales of mixing have been identified and discussed extensively by Baldyga and Bourne (2003). The time and length scales related to macro, meso and micromixing are summarized in Table 1. As an illustration, the calculations of mixing times in a 3L and 20 m^3 reactor from the data published by Larsson et al. (1996), Xu et al. (1999) and Vràbel et al. (2001) were performed. In Table 1, mixing times are calculated using a value of 1.3 kW m^{-3} for ϵ_V which corresponds to a typical value in industrial bioreactors. Since mixing time depends on the turbulent kinetic energy dissipation rate which is not spatially homogeneous in a large reactor, all mixing times in the industrial bioreactor were estimated using two typical values: the volume average value ϵ_V and the value near the injection point often located in the upper part of the reactor below the surface (5% of ϵ_V) (Delafosse, 2008).

Baldyga and Bourne (2003) explained that mixing competes with the reaction as soon as the mixing time is greater than a tenth of the reaction time. From the comparison of mixing times at various scale and biological reaction time (for substrate uptake) one can conclude that

- Whatever the conditions t_E and t_D are actually smaller than a tenth of the smallest assimilation time (0.1 s). Mixing at the microscale (below the Kolmogorov scale) is not a limiting step in bioprocesses. (Note that this information will further be used to compute the uptake rate at the particle from the concentration stored at the node of the DNS grid).
- There is a possible interaction between macromixing (13 s) and substrate assimilation in an industrial bioreactor. This interaction results in the formation of large scale gradients in the bioreactor as reported by Larsson et al. (1996).
- The time scale of mesomixing in an industrial bioreactor is above 0.2 s which is similar to the characteristic time for substrate uptake [0.1–7.5 s]. There is also a real possibility for a mesomixing effect. Moreover, in real systems, the high viscosity of the sirup poured into the reactor probably leads to even higher mixing times. At the labscale, mesomixing is not likely to compete with substrate uptake, unless the experimental device is specifically designed for that as in the work of Amanullah et al. (2001).

These theoretical considerations along with the experimental evidences reported by various authors cited above lead to a

modelling issue which is presented hereafter and constitutes the core of the present paper. When mixing competes with the reaction at a given time scale, a concentration distribution occurs below the corresponding length scale. Typically, if reaction competes with macromixing, the whole reactor can no longer be considered as homogeneous and a compartimentation into smaller zones is necessary. Similarly, if mesomixing competes with assimilation, the spatial resolution of the hydrodynamic model should be increased so that it falls below the integral length scale of concentration fluctuations, Λ. In usual Computational Fluid Dynamic simulations, using the Reynolds Averaged Navier–Stokes equations, the grid size is much larger than Λ and it is necessary to model the effect of subgrid heterogeneity in order to provide a closure model for the (biological) reaction term. This multi-scale modelling methodology is illustrated in Fig. 1.

In the field of chemical reactor engineering, the terminology micro-mixing is used to depict this situation where the characteristic time for mixing is similar or lower than the characteristic reaction time. In this case, the reaction rate is influenced by the dynamics of the mixing process itself. If the relationship between the reaction rate and the concentration is not linear, the actual average reaction rate differs from the reaction rate based on the average concentration. The apparent reaction rate $\langle R(S)\rangle$ is consequently influenced by the dynamics of mixing:

$$R(\langle S\rangle) \neq \langle R(S)\rangle \tag{7}$$

where $\langle . \rangle$ represents a spatial averaging over a volume of control on which mass balances are written. This volume of control is set by the hydrodynamic model used to describe the fluid motion inside the reactor. Therefore, it depends on the spatial resolution of the hydrodynamic model, which can either be the whole reactor, a portion of the reactor (compartment model approach) or a mesh cell (Computational Fluid Dynamics approach). A basic assumption is that concentrations are homogeneous within each volume of control. This implies that the reaction rates are calculated from the averaged concentrations. The present work addresses the following question: what are the consequences of concentration heterogeneities below the resolved scale on the calculation of the biological reaction rates?

3. Modelling the uptake rate distribution

3.1. DNS coupled with Lagrangian tracking of biological phase

The configuration is a homogeneous isotropic turbulent flow. All the fluctuations of the carrier fluid phase and substrate are solved by Direct Numerical Simulation (DNS). This technique ensures that all scales of the turbulence and of the substrate concentration are fully resolved. The computational domain is a 3D box, of length L, with periodic boundary conditions for the fluid velocity and pressure. Statistically turbulent steady flow is obtained with a stochastic spectral forcing proposed by Eswaran and Pope (1988).

The Navier–Stokes equations are coupled with an equation for substrate concentration. The substrate is treated as a passive scalar and the modification of the substrate concentration field by the biological phase is not taken into account. The fluctuations of substrate concentration are produced by an imposed mean gradient of concentration, ζ. Thus the dissipation of substrate concentration by diffusional process is balanced by the production due to the imposed mean gradient. Pandya and Mashayek (2003) and Couzinet et al. (2008) used such an approach for studying non-isothermal particle-laden turbulent flows.

The biological phase is assumed to be composed of spherical microorganisms of diameter of about 1 μm. Then the Stokes number of the suspension is very small so that the microorganisms can be tracked as fluid elements. So the individual trajectories of a large number of microorganisms (200,000) are easily computed from the fluid velocities. For each microorganism n, the assimilation rate, $\Phi(S)^n$, is given by the Monod law (1) using the local concentration of the substrate $S^{(n)}$ at the exact particle location. This concentration is calculated using an accurate interpolation scheme from the Eulerian grid where the substrate concentration and velocity are known.

Such a configuration allows to study the interaction of a biological population with a statistically steady heterogeneous substrate concentration field. The state of each microorganism is only defined by the value of k_S and the maximum specific uptake rate, $q_{S,\max}$, which are assumed constants. Then there is no adaptation of k_S and/or $q_{S,\max}$ to the fluctuations of concentration.

For the present study, several DNS coupled with the Lagrangian tracking of microorganisms have been performed. We have considered two Reynolds number $Re_L = 68$ and $Re_L = 110$, two reference concentrations: $S_0 = 0.15\ \mathrm{kg_S\ m^{-3}}$ and $1\ \mathrm{kg_S\ m^{-3}}$, two imposed gradient: $\zeta = 1\ \mathrm{kg_S\ m^{-4}}$ and $5\ \mathrm{kg_S\ m^{-4}}$, and three affinity constants $k_S = 10^{-3}\ \mathrm{kg_S\ m^{-3}}$, $10^{-1}\ \mathrm{kg_S\ m^{-3}}$ and $10^{2}\ \mathrm{kg_S\ m^{-3}}$. Beyond these practical values it must be noticed that the relevant parameters are the ratio $k_S/\langle S\rangle$ and the reference concentration S_0. The local turbulent energy dissipation rates are $\epsilon = 0.0163\ \mathrm{m^2\ s^{-3}}$ and $\epsilon = 0.15\ \mathrm{m^2\ s^{-3}}$ for $Re_L = 68$ and $Re_L = 110$ respectively. Thus the local energy dissipation rates considered here correspond to those observed far from the impeller in a stirred tank where the mean specific power input are $\epsilon_V = 0.26\ \mathrm{kW\ m^{-3}}$ and $\epsilon_V = 3\ \mathrm{kW\ m^{-3}}$.

3.2. PDF of substrate concentration seen by microorganisms

The goal of this section is to derive a theoretical distribution of the substrate concentration. In the frame of the assumptions described in previous section, the substrate concentration is decomposed as

$$S = S_0 + s_g + s' \tag{8}$$

with s_g the contribution from the imposed gradient, S_0 the reference concentration and s' the fluctuating concentration. Assuming that the fluctuating part follows a Gaussian distribution and that the microorganisms are uniformly randomly distributed in the domain, the distributions of each variable of (8) write

$$P(s) = \delta(s - S_0), \tag{9}$$

$$P(s') = \frac{1}{\sqrt{2\pi}\sqrt{\langle s'^2\rangle}} \exp\left(-\frac{1}{2}\frac{s'^2}{\langle s'^2\rangle}\right), \tag{10}$$

$$P(s_g) = \begin{cases} \frac{1}{\zeta L} & \text{if } -\zeta\frac{L}{2} \le s_g \le \zeta\frac{L}{2} \\ 0 & \text{otherwise} \end{cases}. \tag{11}$$

These three contributions are shown in Fig. 2. We emphasize that the three distributions are independent because, by construction, s' and s_g are not correlated. The distribution of the substrate concentration is a combination of the three individual distributions. More specifically, it is defined as the convolution of the three distributions and yields to $P_S(S) = P(s) * P(s') * P(s_g)$. From (9) to (11) and through the convolution, the substrate concentration distribution writes

$$P_S(S) = \frac{1}{2\zeta L}\left[\mathrm{erf}\ \frac{S - S_0 + \zeta L/2}{\sqrt{2\langle s'^2\rangle}}\right) - \mathrm{erf}\ \frac{S - S_0 - \zeta L/2}{\sqrt{2\langle s'^2\rangle}}\right)\Bigg] \tag{12}$$

where $\mathrm{erf}(x)$ is the error function defined by

$$\mathrm{erf}(x) = \frac{2}{\sqrt{\pi}} \int_0^x \mathrm{e}^{t^2/2}\, dt. \tag{13}$$

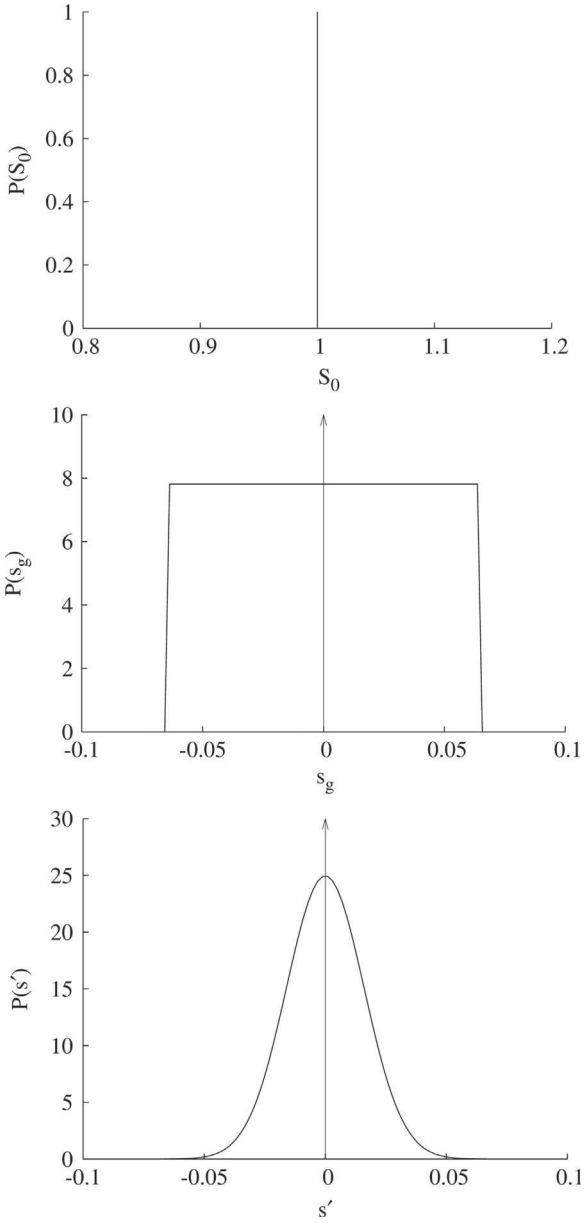

Fig. 2. Theoretical decomposition of the substrate concentration as a reference concentration (top), a gradient contribution (middle) and a Gaussian fluctuation (bottom).

The distribution functions P_S are shown in Fig. 3 for two concentration gradients. Note that the scale of the horizontal axis is different for the two panels and that the minimum value is not zero. In both cases, the reference concentration of substrate $S_0 = 1.0\ \mathrm{kg_S\ m^{-3}}$. It can be observed that, as expected, the width of the concentration distribution increases with the mean gradient. Even if some small differences are present we observe that the theoretical modelling of the substrate concentration distribution is in correct agreement with the DNS results for two mean concentration gradients.

We can conclude that the analytical distribution for the total substrate concentration presented in Eq. (12) is a general form that depends on the imposed gradient, the length of the domain, the mean imposed concentration and the substrate concentration variance. The latter is dependent on the Reynolds number so that the effect of mixing is implicitly included in the distribution.

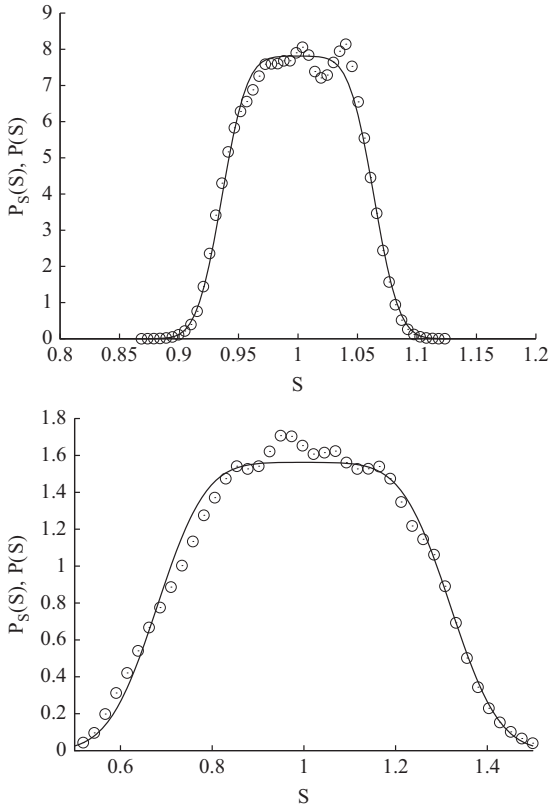

Fig. 3. Comparison of the analytical distribution for the instantaneous concentration S (——) given by (12) with the distribution from DNS simulations (○). Case where reference concentration of substrate $S_0 = 1.0\ \mathrm{kg_S\ m^{-3}}$. In top panel, the imposed mean concentration gradient is $\zeta = 1\ \mathrm{kg_S\ m^{-4}}$ and in bottom panel $\zeta = 5\ \mathrm{kg_S\ m^{-4}}$.

3.3. Derivation of the mass flux distribution

From the distribution of substrate concentration it is now possible to derive the distribution of the uptake rate $\hat{q}$ for the biological suspension. As for the DNS we assume that the Monod law (1) is valid. Then the normalized uptake rate $\hat{q}$ writes

$$\hat{q} = \frac{q_S}{q_{S,max}} = \frac{S}{S + k_S}. \tag{14}$$

We emphasize that the following methodology is applicable to another assimilation model. As the mass flux directly depends on the substrate concentration a theoretical solution exists for the determination of the mass flux distribution. Assuming that the assimilation rate is given in terms of substrate concentration by a function $R(S)$, the distribution of the mass flux writes

$$P_{\hat{q}}(\hat{q}) = \frac{1}{R'[R^{-1}(S)]} P_S(R^{-1}(S)). \tag{15}$$

where on the right-hand-side the distribution function P_S is given by (12). Also in (15), R' is the first derivative of the function R. The inverse function R^{-1} is thus given by $R^{-1}(x) = k_S x/(1-x)$ if $x \neq 1$. By definition of Monod assimilation model, the curve $x=1$ is the asymptote of $\hat{q}$ so that the previous inverse function is defined for all $\hat{q}$. Then in the case of Monod assimilation law, the distribution function for the non-dimensionalized mass flux becomes

$$P_{\hat{q}}(\hat{q}) = \frac{k_S}{(1-\hat{q})^2} P_S\left(\frac{k_S \hat{q}}{1-\hat{q}}\right). \tag{16}$$

For model assessment we first compare our theoretical derivation with DNS results in cases where the substrate concentration distribution obeys a Gaussian distribution. In other words, the

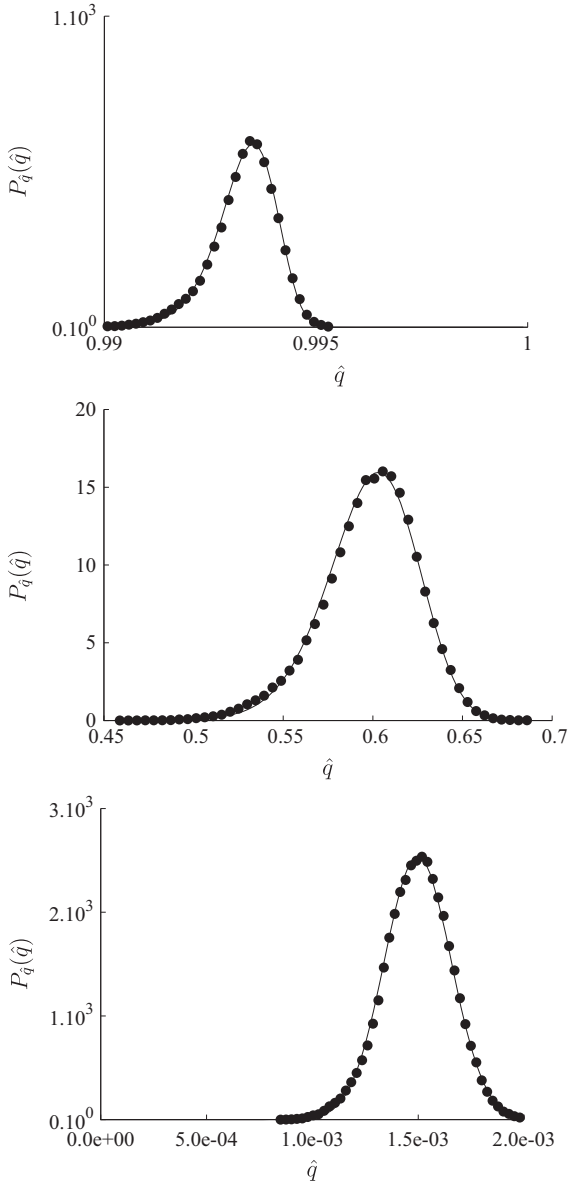

Fig. 4. Comparison of the analytical distribution for the assimilated mass flux by the microorganisms (——), and given by (17), with the distribution measured from DNS (●) without the contribution of the substrate gradient for the assimilation rate. Case with $S_0 = 0.15\ \mathrm{kg_S\ m^{-3}}$ and $\zeta = 1\ \mathrm{kg_S\ m^{-4}}$. Top panel: $k_S = 10^{-3}\ \mathrm{kg_S\ m^{-3}}$, middle: $k_S = 10^{-1}\ \mathrm{kg_S\ m^{-3}}$ and bottom: $k_S = 10^{2}\ \mathrm{kg_S\ m^{-3}}$.

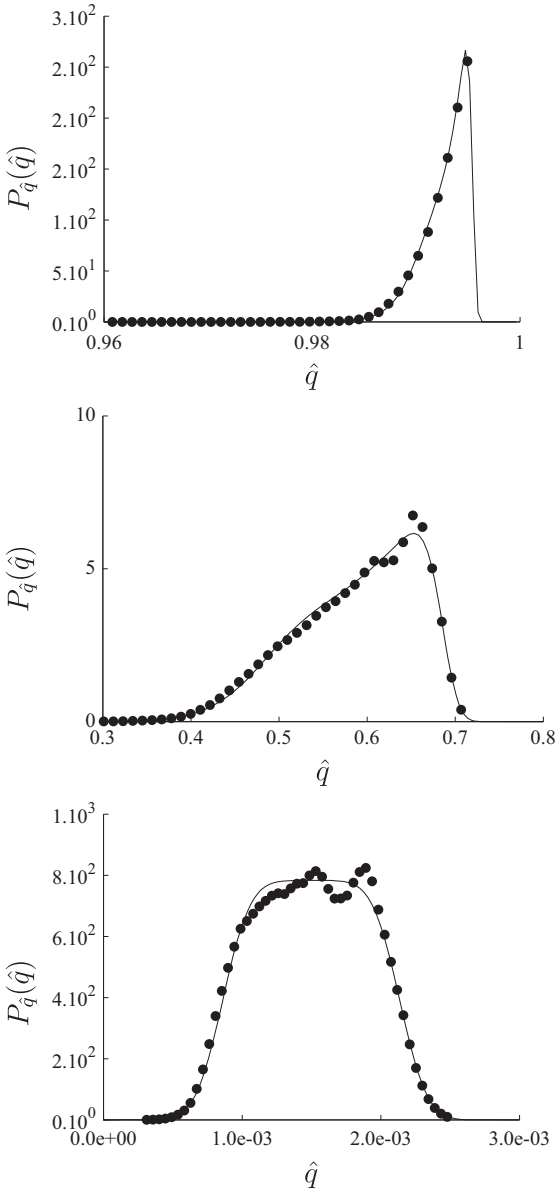

Fig. 5. Comparison of the analytical distribution for the assimilated mass flux by the microorganisms (——), and given by (18), with the distribution measured from DNS (●). Case with $\zeta = 1\ \mathrm{kg_S\ m^{-4}}$ and $S_0 = 0.15\ \mathrm{kg_S.m^{-3}}$. Top panel: $k_S = 10^{-3}\ \mathrm{kg_S\ m^{-3}}$, middle: $k_S = 10^{-1}\ \mathrm{kg_S\ m^{-3}}$ and bottom: $k_S = 10^{2}\ \mathrm{kg_S\ m^{-3}}$.

gradient contribution is not taken into account in the uptake rate calculation. Then, and according to previous considerations, the following equation is found for the mass flux distribution:

$$P_{\hat{q}}(\hat{q}) = \frac{k_S}{(1-\hat{q})^2}\frac{1}{\sqrt{2\pi\langle s'^2\rangle}} \times \exp\left[\frac{k_S^2}{2\langle s'^2\rangle}\left(\frac{\hat{q}}{1-\hat{q}} - \frac{S_0}{k_S}\right)^2\right]. \tag{17}$$

The results are presented in Fig. 4 for the case with $S_0 = 0.15\ \mathrm{kg_S\ m^{-3}}$ and for several values of the affinity constant. Here again and for sake of readability the scale of the horizontal axis is different for each graph. The calculated distribution and the analytical evolution for the uptake rate distribution are in very good accordance. The obtained distributions seem nearly Gaussian. Nevertheless asymmetric evolutions are observed at both extremities of the distribution. These graphs illustrates the fact that, in the same environment, the actual mass flux distribution depends on the affinity constant of the cells. The flux is almost maximum for all cells if $k_S \ll S_0$ (top panel), around a thousandth of this maximum if $k_S \gg S_0$ (bottom panel) and the most significant differences among the population will be obtained in the case $k_S \approx S_0$ (middle panel).

Then, we consider the general case where the substrate gradient affects the mass flux distribution. The corresponding substrate concentration distribution $P_S(S)$ is given by (12). Using Monod assimilation model, the mass flux distribution is now given by

$$P_{\hat{q}}(\hat{q}) = \frac{k_s}{(1-\hat{q})^2}\frac{1}{2\zeta L} \times \left[\mathrm{erf}\left(\frac{\frac{k_S\hat{q}}{1-\hat{q}} - S_0 + \zeta L/2}{\sqrt{2\langle s'^2\rangle}}\right) - \mathrm{erf}\left(\frac{\frac{k_S\hat{q}}{1-\hat{q}} - S_0 - \zeta L/2}{\sqrt{2\langle s'^2\rangle}}\right)\right]. \tag{18}$$

The analytical and calculated distributions for three different affinity constants are shown in Fig. 5. In all cases the two

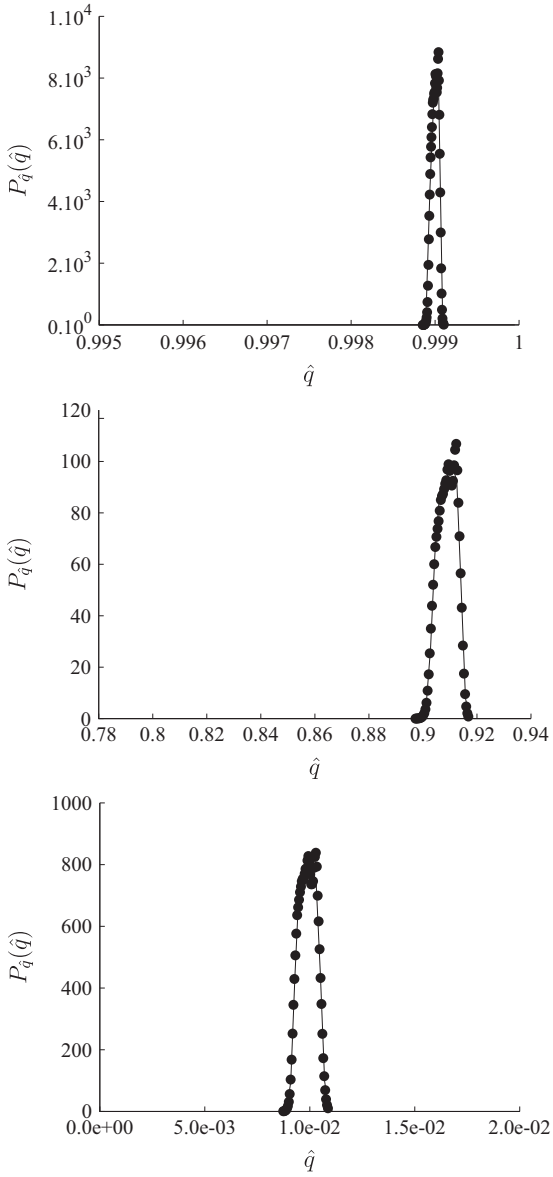

Fig. 6. Comparison of the analytical distribution for the assimilated mass flux by the microorganisms (—mdash), and given by (18), with the distribution measured from DNS (•). Case with $\zeta = 1\ \mathrm{kg_S\ m^{-4}}$ and $S_0 = 1\ \mathrm{kg_S\ m^{-3}}$. Top panel: $k_S = 10^{-3}\ \mathrm{kg_S\ m^{-3}}$, middle: $k_S = 10^{-1}\ \mathrm{kg_S\ m^{-3}}$ and bottom: $k_S = 10^{2}\ \mathrm{kg_S\ m^{-3}}$.

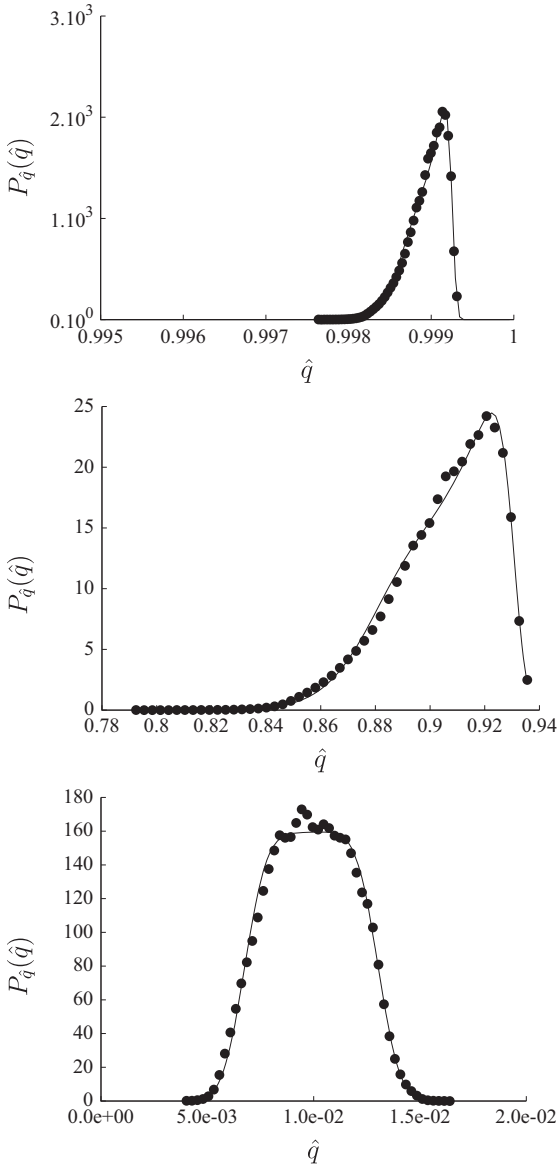

Fig. 7. Comparison of the analytical distribution for the assimilated mass flux by the microorganisms (——), and given by (18), with the distribution measured from DNS (•). Case with $\zeta = 5\ \mathrm{kg_S\ m^{-4}}$ and $S_0 = 1\ \mathrm{kg_S\ m^{-3}}$. Top panel: $k_S = 10^{-3}\ \mathrm{kg_S\ m^{-3}}$, middle: $k_S = 10^{-1}\ \mathrm{kg_S\ m^{-3}}$ and bottom: $k_S = 10^{2}\ \mathrm{kg_S\ m^{-3}}$.

distributions are in a close agreement. The mass flux distribution on the top graph is very narrow which indicates that the heterogeneity of the concentration field has almost no consequences on the mass flux distribution as soon as $S_0 \gg k_S$. This corresponds to a first asymptotic behavior: for any particle, $\hat{q} \simeq 1$ when S/k_S goes to zero. In this case, which can therefore be referred as non-limiting conditions, the uptake capacity of all cells is saturated. On the bottom graph, it is observed that the mass flux distribution has the same shape as the substrate concentration distribution (see Fig. 3). This is due to the linear relationship between the flux and the concentration for $S \ll k_S$. This constitutes another asymptotic behavior: $\hat{q} \simeq S/k_S$ is verified for large k_S/S, i.e, when the substrate concentration is limiting. Thus when the relationship between the uptake rate and the concentration is linear (at high and low S/k_S). The mass flux distribution is easily obtained from the concentration distribution. In the midrange, the flux distribution is not easily predictable because the different parameters (substrate concentration variance, affinity constant, mean substrate concentration, and gradient contribution) directly affect the mass flux distribution. If the mean concentration and the affinity constant are of the same order of magnitude, the symmetry of the concentration distribution is lost when one moves to the mass flux distribution. The mass flux distribution does not resemble the substrate concentration distribution and it is then essential to take into account the concentration gradient. It is noteworthy that many biological processes are operated under a substrate limitation, meaning that $S/k_S \simeq 1$.

The effect of the magnitude of the gradient on the mass flux distribution is presented in Figs. 6 and 7. The mean concentration is $S_0 = 1\ \mathrm{kg_S\ m^{-3}}$ resulting in larger ratios S/k_S than in the situation depicted in Fig. 5, the mass flux distributions are consequently much narrower. As expected, increasing the magnitude of the gradient results in wider mass flux distributions. This is true for all situations but once again, the most interesting case is presented in the middle graph. The parameters are such that the mean concentration is ten times larger than the affinity constant. So the average mass flux based on the mean concentration would be around 10/11 of its maximum value. Note that all distributions

are effectively centered on the mean value that would be calculated from the mean concentration. Yet, the width of the mass flux distributions is larger in Fig. 7 where the gradient is five time that in Fig. 6. All these results indicate that the consequences of substrate heterogeneities are effective on the mass flux distribution as soon as one enters the range $S/k_S < 10$ and that they are most significant in the case $S/k_S \approx 1$. Moreover increasing the magnitude of the concentration gradient increases the heterogeneity of the substrate concentration fields which in turn results in wider mass flux distributions.

Through an analytical approach, the local concentration heterogeneities seen by the individual microorganisms of a given population (characterized by the affinity constant k_S) can be integrated at the population scale in order to produce a mass flux distribution. This result is obtained when an assimilation law is prescribed at the microorganism scale and when assimilation itself does not influence the substrate concentration field. Now the consequences in terms of microbial productions can be examined through the consideration of a basic metabolic model.

4. Metabolic model

4.1. Metabolic model

The metabolic model is adapted from that published by Xu et al. (1999) for *Escherichia coli* in batch or fed-batch cultivations under fully aerobic conditions. It is based on a limited number of key internal processes (or reactions) as well as mass and energy balances:

- Anabolism

$$S + Y_{SE} ATP \xrightarrow{q_{ana}} Y_{SX} X \tag{19}$$

- Oxidative catabolism

$$S + Y_{SO} O_2 \xrightarrow{q_{oxy}} Y^o_{SE} ATP \tag{20}$$

- Fermentary catabolism

$$S \xrightarrow{q_{ferm}} Y_{SP} P + Y^f_{SE} ATP \tag{21}$$

- Dissimilation

$$S + ATP \xrightarrow{q_{over}} Y_{SBP} \tag{22}$$

- Maintenance

$$ATP \xrightarrow{q_{main}} 0 \tag{23}$$

where q_α are the specific rates of intracellular reactions in $\mathrm{mol_S\ g_X^{-1}\ h^{-1}}$, and Y_{ij} are the stoichiometric coefficients in $\mathrm{mol_j\ mol_i^{-1}}$. The upper script stands for oxidative or fermentary catabolism.

In the case of facultative aerobes, energy can be obtained from an oxidative pathway or by fermentation when oxygen is absent or in default. The two metabolic pathways do not have the same energetic yield and fermentary catabolism leads to the formation of a product *P*. It is assumed that *overflow* metabolism leads to the excretion of another by-product named *BP* (for BioPolymer). The production of new cellular material (anabolism), the withdrawal of carbon in excess (dissimilation or *overflow* metabolism) and maintenance are energy consuming.

Table 2
Parameter values of the metabolic model of *Escherichia coli*.

Name	Symbol	Value	Unit
Anabolism (ATP)	Y_{SE}	12.05	$[\mathrm{mol_{ATP}\ mol_S^{-1}}]$
Anabolism (biomass)	$Y_{XS}M_X$	136.6	$[\mathrm{g_X\ mol_S^{-1}}]$
Oxidative catabolism (oxygen)	Y_{SO}	6.0	$[\mathrm{mol_{O2}\ mol_S^{-1}}]$
Oxidative catabolism (ATP)	Y^o_{SE}	20.0	$[\mathrm{mol_{ATP}\ mol_S^{-1}}]$
Fermentary catabolism (product)	Y_{SP}	6.0	$[\mathrm{mol_P\ mol_S^{-1}}]$
Fermentary catabolism (ATP)	Y^f_{SE}	3.0	$[\mathrm{mol_{ATP}\ mol_S^{-1}}]$
Dissimilation (biopolymer)	Y_{SBP}	1.0	$[\mathrm{mol_{BP}\ mol_S^{-1}}]$

The specific reaction rates, r_i, expressed in $[\mathrm{g_i\ g_X^{-1}\ h^{-1}}]$, are given by the following set of equations:

$$r_X = q_{ana}.Y_{SX}.M_X \tag{24}$$

$$r_{O2} = -q_{oxy}.Y_{SO}.M_{O2} \tag{25}$$

$$r_S = -(q_{ana} + q_{oxy} + q_{ferm} + q_{over}).M_S \tag{26}$$

$$r_P = q_{ferm}.Y_{SP}.M_P \tag{27}$$

$$r_{BP} = q_{over}.Y_{SBP}.M_{BP} \tag{28}$$

where M_i are the molar masses of the different species. Table 2 gathers the different parameters of the metabolic model.

4.2. Calculation of the metabolic fluxes – hypothesis

In order to get the production or consumption term in the conservation equation of a given species, the intracellular rates have to be calculated for each value of the uptake rate considering the actual distribution experienced by the microbial population. Before that, some simplification are made.

1. *No accumulation*: assuming that neither energy nor mass accumulate inside the microorganisms the following conservation equation for energy (namely ATP) over the cell can be written as

$$q_{oxy} Y^o_{SE} + q_{ferm} Y^f_{SE} - q_{ana} Y_{SE} - q_{over} - q_{main} = 0. \tag{29}$$

   A conservation equation for the substrate can be obtained by equating the total specific molar flux through the cell membrane q_S $[\mathrm{mol_S.g_X^{-1}.h^{-1}}]$ to the sum of all intracellular substrate consumption rates:

$$q_S = q_{ana} + q_{oxy} + q_{over} + q_{ferm}. \tag{30}$$

2. *Preferential catabolism*: the bacteria are supposed to favor the production of energy through the oxidative pathway and they only make use of the fermentation pathway when the amount of energy produced by oxidation does not fulfill the energetic demand.
3. *Overflow metabolism*: the excretion of carbon in excess is triggered when the rate of substrate assimilation is greater than the rate of consumption due to anabolism and catabolism. The amount of energy consumed by the dissimilation is supposed to be negligible which results in the elimination of q_{over} in (29).
4. *Maintenance*: the energetic cost of maintenance is supposed to be negligible which also leads to a simplification of (29).
5. *Oxygen consumption rate*: in the metabolic model, the oxygen consumption rate is a function of the local dissolved oxygen concentration in the liquid phase. In the following, it is

assumed that the dissolved oxygen concentration is homogeneous down to the particle scale and non-limiting, such that only oxidative catabolism is active. This simplification allows a direct calculation of all metabolic fluxes, since the mass balance for the substrate can be simplified as follows:

$$q_S = q_{ana} + q_{oxy} + q_{over}, \tag{31}$$

and the energy balance now reduces to

$$q_{ana} Y_{SE} = q_{oxy} Y^o_{SE}. \tag{32}$$

We note that it would be also possible to proceed to the resolution of the metabolic model in case of oxygen limitation. In the context of this work it would necessitate a joint distribution function for the substrate and oxygen mass fluxes. Since this information is not available at the moment, oxygen non-limiting conditions are assumed.

6. *Relation between fluxes and internal reaction rates*: dividing Eq. (31) by $q_{S,\max}$ form the non-dimensional variable $\hat{q}$, see Eq. (14), for which we have derived the theoretical distribution (18). The normalized internal reaction rates that appear on the right side of Eq. (31) will therefore depend on both the concentration distribution and the type of microorganisms considered (identified by the value of k_S).

4.3. Metabolic fluxes at equilibrium

In the original model of Xu et al. (1999), the overflow metabolism starts under fully aerobic conditions when the rate of oxygen consumption required for glucose oxidation exceeds the maximum respiration rate. In that case, the uptaken substrate flux exceeds the maximum oxidative capacity of the cell. In the present work, a slightly different approach is used. It is assumed here that overflow metabolism is triggered when the instantaneous substrate uptake rate exceeds the rate of substrate utilization through anabolism and oxidative catabolism pathways. Since statistically steady simulations are performed, the averaged concentration S_0 is constant. Although the population of cells is transported in a heterogeneous medium it is reasonable to consider that each cell functioning is adapted to the averaged concentration. The cell abilities in terms of anabolism and catabolism are assumed to be at equilibrium with the average concentration. Equivalently, it means that the characteristic time of cell metabolism adaptation is much larger than the characteristic time of concentration fluctuations along the cell trajectory. In other words, the metabolism is balanced (without overflow) when the assimilation rate equals the utilization rate corresponding to the mean concentration S_0. In any other case a cell can be considered as out of equilibrium: receiving a substrate flux that does not matches its needs (Morchain et al., 2014). In the following, this equilibrium state is marked by the superscript "0". In the state of equilibrium, the assimilation rate exactly meets the sum of utilization rates through the anabolic and oxidative catabolic pathways. Using non-dimensional variables, this leads to

$$\hat{q}^0 = \frac{S_0}{k_S + S_0} = \hat{q}^0_{ana} + \hat{q}^0_{oxy}. \tag{33}$$

The simplified energy balance presented in the previous section gives

$$\hat{q}_{oxy} = \frac{Y_{SE}}{Y^o_{SE}} \hat{q}_{ana} = \alpha\, \hat{q}_{ana}, \tag{34}$$

which is also valid in the balanced growth state, therefore we get

$$\hat{q}^0_{ana} = \frac{1}{1+\alpha} \hat{q}^0, \tag{35}$$

$$\hat{q}^0_{oxy} = \frac{\alpha}{1+\alpha} \hat{q}^0. \tag{36}$$

4.4. Metabolic fluxes out of equilibrium

The determination of the actual metabolism in the general case is based on the comparison between the normalized uptake rate $\hat{q}$ and the normalized utilization rate at equilibrium $\hat{q}^0$.

On the one hand, microorganisms receiving a substrate flux $\hat{q}$ smaller than $\hat{q}^0$ are facing a nutrient limitation. As explained in the previous paragraph, all cells are accustomed to an average flux $\hat{q}^0$ meaning that the *cell factory* would be able to metabolize larger amounts of substrate. As a consequence the totality of the substrate assimilated is directed to the anabolic and oxidative catabolic pathways. Eqs. (35) and (36) remain valid since the proportionality between q_{oxy} and q_{ana} is maintained. The only difference is that the superscript "0" falls indicating that the actual reaction rates are sub-optimal.

$$\hat{q}_{ana} = \frac{1}{1+\alpha} \hat{q}, \tag{37}$$

$$\hat{q}_{oxy} = \frac{\alpha}{1+\alpha} \hat{q}. \tag{38}$$

On the other hand, the sub-population exposed to substrate concentrations larger than S_0 internalize a substrate flux $\hat{q}$ larger than $\hat{q}^0$ and they have to cope with an excess of nutrient. The anabolic and catabolic capacities of those cells are saturated and therefore equal the equilibrium values:

$$\hat{q}_{ana} = \frac{1}{1+\alpha} \hat{q}^0, \tag{39}$$

$$\hat{q}_{oxy} = \frac{\alpha}{1+\alpha} \hat{q}^0. \tag{40}$$

The amount of substrate directed in the anabolic and oxidative catabolic pathways are thus upperbounded by the values at equilibrium. These are related to the average concentration and constitute local maxima for the substrate utilization rate. As a consequence, the difference between the effective uptake rate and the utilization rate represents an extra-assimilation which has to be diverted into by-products since accumulation is not allowed in the metabolic model.

The number of moles of by-product formed depends on the stoichiometry of the reaction converting internal substrate into by-products. For the sake of convenience it will be assumed here that the stoichiometric coefficient Y_{SBP} is equal to unity, this also implies $M_S = M_{BP}$ and we will analyze the results in terms of $\hat{q}_{over}$ defined as

$$\hat{q}_{over} = \frac{q_{over}}{q_{S,max}} = \hat{q} - \hat{q}^0. \tag{41}$$

4.5. Population averaged bioreaction rates

By definition the mean substrate consumption rate (averaged over the population of microorganisms) is the first moment of the uptake rate distribution $P_{\hat{q}}(\hat{q})$. In a practical way, we calculate the normalized value of the mean substrate consumption rate (the mean divided by $q_{S,max}$):

$$\langle \hat{q} \rangle = \int_0^\infty \hat{q}\, P_{\hat{q}}(\hat{q})\, d\hat{q}. \tag{42}$$

It is shown on the top panel of Fig. 8 that, in any situation investigated numerically, the mean substrate consumption rate is very close to that computed from the mean concentration S_0, so we have $\langle \hat{q} \rangle = \hat{q}^0$. In fact, some small differences between $\langle \hat{q} \rangle$ and $\hat{q}^0$, are found, as shown in the bottom panel of figure. These are

due to the nonlinearity of (1), but they represent, in the worst case, less than one percent. This is a very important result which shows that, despite the presence of concentration heterogeneities and the non-linearity of the relationship $q = f(S)$, the mean concentration value is relevant to compute the overall substrate consumption rate.

However, it was shown previously that, in a heterogeneous medium, some cells are exposed to a nutrient limitation while some others are simultaneously facing an excess of nutrient. Thus, in our approach it is admitted that some cells can internalize more substrate than the whole population does on average. Nevertheless, the global substrate consumption is not affected. Recall that in standard approaches ignoring small scale heterogeneities, the uptake rate of the entire population is uniquely defined from the mean concentration.

The population averaged or mean specific growth rate is related to the mean anabolic rate through (24). This leads to the following expression for the mean normalized specific growth rate:

$$\langle \hat{\mu} \rangle = \frac{\langle \mu \rangle}{\mu_{max}} = \int_0^\infty \hat{q}_{ana}(\hat{q}) P_{\hat{q}}(\hat{q})\, d\hat{q}. \tag{43}$$

The relative specific growth rate $\langle \hat{\mu} \rangle$ can be compared to the relative specific growth rate $\langle \hat{\mu}^0 \rangle$ that would be obtained if the same flux was assimilated by each particle in the box (perfectly mixed assumption). The latter can be expressed as

$$\langle \hat{\mu}^0 \rangle = \int_0^\infty \frac{\hat{q}^0}{1+\alpha} P_{\hat{q}}(\hat{q})\, d\hat{q} = \frac{1}{1+\alpha}\hat{q}^0. \tag{44}$$

The integration interval of (43) must be split into two subintervals because the definition of $\hat{q_{ana}}(\hat{q})$ depends on the value of $\hat{q}$ with respect to $\hat{q}^0$:

$$\frac{\langle \hat{\mu} \rangle}{\langle \hat{\mu}^0 \rangle} = \frac{1+\alpha}{\hat{q}^0}\left[\int_0^{\hat{q}^0} \frac{\hat{q}}{1+\alpha} P_{\hat{q}}(\hat{q})\, d\hat{q} + \int_{\hat{q}^0}^\infty P_{\hat{q}}(\hat{q}) \frac{\hat{q}^0}{1+\alpha} d\hat{q}\right]. \tag{45}$$

The first term on the right-hand-side corresponds to the growth limited by the incoming flux (physical limitation) and the second term corresponds the growth limited by the cell capacities (biological limitation). Recall that the mean anabolic flux is the same for all cells and defined by S_0. The ratio $\langle \hat{\mu} \rangle / \langle \hat{\mu}^0 \rangle$ therefore quantifies the specific growth rate reduction due to imperfect mixing.

4.6. By-product formation

Following the same approach, the mean normalized production rate of by-product due to overflow metabolism is obtained through

$$\langle \hat{q}_{over} \rangle = \frac{1}{\hat{q}^0} \int_{\hat{q}^0}^\infty \left(\hat{q} - \hat{q}^0\right) P(\hat{q})\, d\hat{q}. \tag{46}$$

It corresponds to the ratio between the mean by-product formation rate and the mean substrate consumption rate. It can also be interpreted as the fraction of the total substrate influx that is diverted towards overflow metabolism. Normalized distribution of the normalized flux $\hat{q}$ is measured in numerical simulations. As already explained, simulations are performed with the same averaged concentration S_0 for various type of microorganisms distinguished by their own affinity constant k_S. Different values of k_S were investigated, which implies that the values of $\hat{q}^0$ were also different.

5. Results and discussion

In this first part of the results, calculations are performed with an averaged concentration $S_0 = 0.15\ \mathrm{kg_S\ m^{-3}}$, a concentration gradient $\zeta = 1\ \mathrm{kg_S\ m^{-4}}$ and a Reynolds number of 110. These parameters determine the substrate concentration field. A value of $k_S = 0.1\ \mathrm{kg_S\ m^{-3}}$ is chosen to calculate the associated uptake rate distribution which is presented in upper panel of Fig. 9. The mean value $\langle \hat{q} \rangle = \hat{q}^0$ is equal to 0.6 under these conditions. Subsequently, Eqs. (33)– (41) are used to quantify the internal metabolic rates for any possible value of $\hat{q}$. Results are presented in the lower panel of Fig. 9. It can be observed that the rates of anabolism and oxidative catabolism are proportional, both increasing with $\hat{q}$, as long as $\hat{q} \le \hat{q}^0$. Beyond this limit, the rates of anabolism and oxidative catabolism remain constants while the rate of overflow metabolism progressively increases.

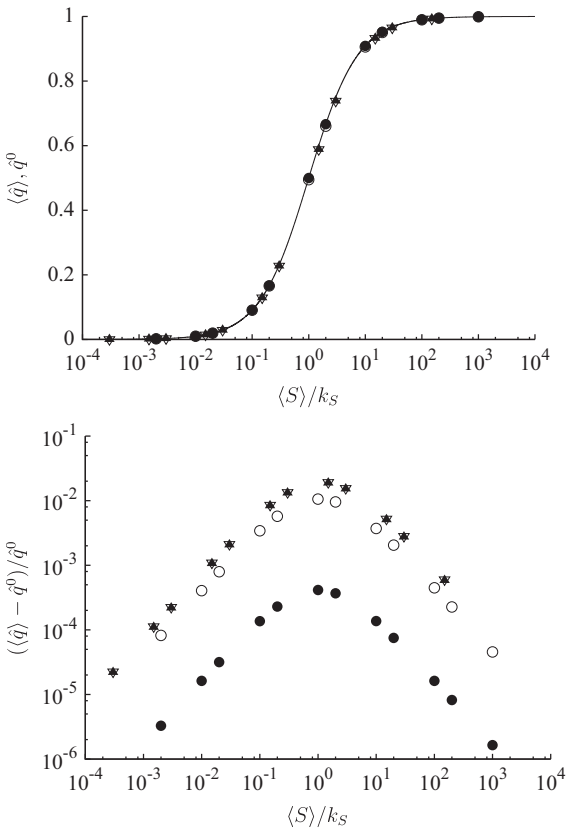

Fig. 8. Normalized average uptake rates (top), $\langle \hat{q} \rangle$ (symbols) population average, $\hat{q}^0$ (continuous line) computed from the average concentration and relative error (bottom) measured in all numerical simulations.

It can be noticed that these calculations only depend on the value of $\hat{q}$ and $\hat{q}^0$ that defines the limit between limited growth and over-flow metabolism. These calculations can be conducted *a priori* using any predictive metabolic model.

The overall consequences in terms of specific growth rate and by-product formation for the entire population actually result from the combination of the two graphs presented in Fig. 9. The exact mathematical expression was given in Eqs. (45) and (46). From these graphs, it is clear that if one considers two concentration fields characterized by the same average concentration, the mean rates computed from the aforementioned equations will be dependent on the exact shape of the substrate concentration distribution. Moreover, if one considers the same concentration field but different affinity constants for the substrate, apparent reaction rates will also be impacted. The quantification of these aspects is treated in the following paragraphs.

Fig. 10 presents the normalized specific growth rate and the fraction of the incoming substrate flux diverted into by-product for different values of the ratio S_0/k_S. The calculations of integrals corresponding to were performed using the same scalar field for

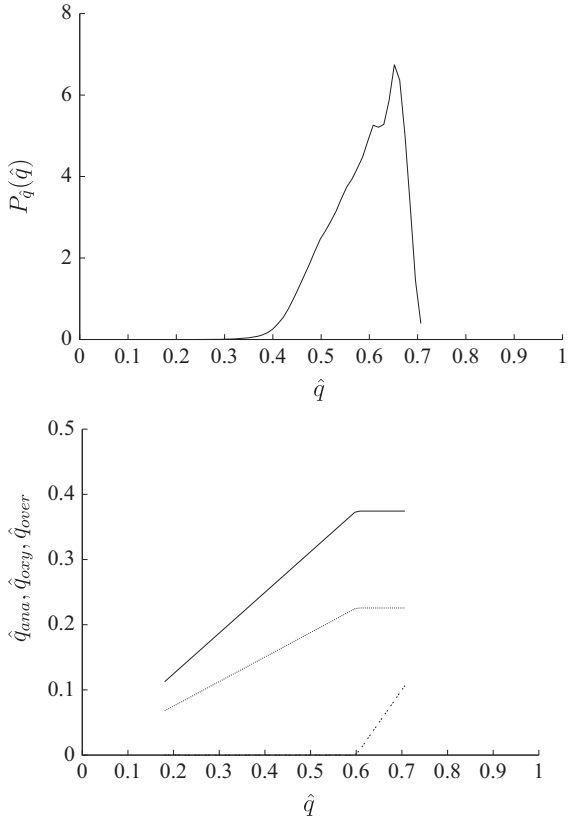

Fig. 9. Normalized uptake rate distribution (top) and corresponding anabolism (continuous line), oxidative catabolism (dotted line) and overflow (dashed line) rates with respect to the normalized uptake rate for the case where $\zeta = 1\ \mathrm{kg_S\ m^{-4}}$ and $S_0 = 0.15\ \mathrm{kg_S\ m^{-3}}$.

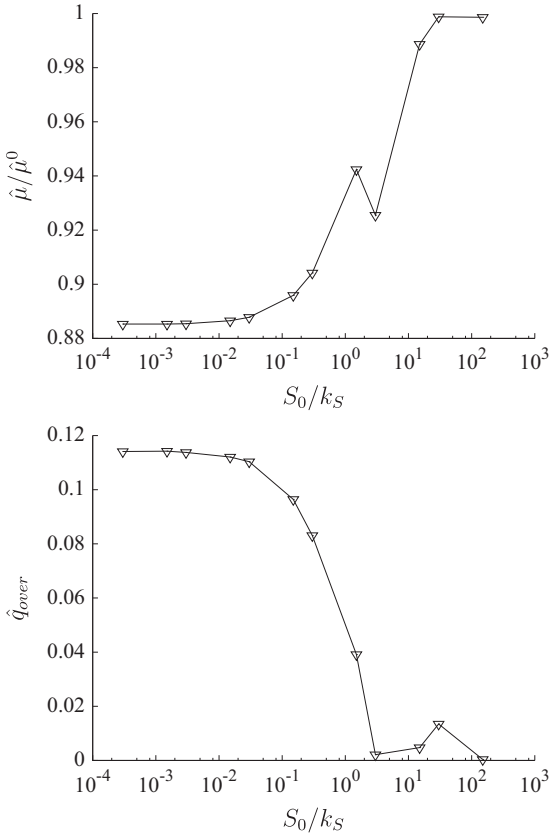

Fig. 10. Specific growth rate reduction and by-products formation with respect to the ratio $\langle S \rangle / k_S$ for the case where $\zeta = 1\ \mathrm{kg_S\ m^{-4}}$ and $S_0 = 0.15\ \mathrm{kg_S\ m^{-3}}$.

different values of k_S. On the right-part of the graphs, the affinity constant for the substrate is much smaller than the average concentration, the uptake capacity is saturated, the uptake rate is maximum and consequently the presence of concentration gradient has almost no effect on the mean population growth rate (which is indeed equal to $\mu_{\max}$). In fact, the distribution $P(\hat{q})$ is also very narrow and since $\hat{q}^0 \to 1$, no by-product is formed. On the left-part of the graphs, the distribution of S results in a distribution of $P(\hat{q})$ such that $\hat{q}^0 \ll 1$ so the whole population is growing at $\mu < \mu_{max}$. Among this population some individuals are facing limiting conditions, those for which $\hat{q} < \hat{q}^0$, some other individuals have to cope with an excess of substrate $\hat{q} > \hat{q}^0$. Thus, we concomitantly observe a reduced growth rate and a by-product formation at the population scale. In this zone of severe limitation, it is found that the specific growth rate reduction becomes independent of the ratio S/k_S. This asymptotic behavior at very low values of the parameter $\langle S \rangle / k_S$ can be related to the linear relationship between S and q_S. First of all, recall that the variable $1 - \langle \hat{\mu} \rangle / \langle \hat{\mu}^0 \rangle$ represents the growth rate reduction with respect to the maximum value that would be obtained under perfectly mixed conditions. Then, considering Eq. (45), one observes that the reduction of the growth rate is due to the left-part of the mass flux distribution (that below $\hat{q}^0$). Thus it depends on the sole shape of the uptake rate distribution.

Secondly, it was shown that the concentration distribution is nearly Gaussian and that the mass flux distribution is very similar to the concentration distribution at low S/k_S. This explains why an asymptotic behavior is observed.

As already explained, it is expected that both the magnitude of the gradient and the energy dissipation rate (related to the Reynolds number) determine the asymptotic value since they have a major effect on the width of the mass flux distribution. In Fig. 11, the specific growth rate reduction is presented as a function of the ratio $\langle S \rangle / k_S$ for the different flow configurations (resulting in different concentration distributions). For all flow configurations, the same trend is observed: a growth rate reduction is present for small values of the ratio S_0/k_S (i.e. under substrate limiting conditions). The magnitude of this phenomenon depends on the heterogeneity of the substrate concentration field. The simulation with $Re = 110$, $\zeta = 0.1\ \mathrm{kg_S\ m^{-4}}$, and $S_0 = 1.0\ \mathrm{kg_S\ m^{-3}}$, represented by the black-filled bullet ●, leads to a narrow distribution and consequently, there is almost no drop in the specific growth rate. Increasing the magnitude of the concentration gradient while preserving the same average concentration and velocity fields (○) produces a more heterogeneous concentration field. As a result, the fraction of cells facing sub-optimal concentrations increases and the actual specific growth rate is lower than what it would be in a perfectly mixed environment. In the end, simulations ▲ and ▽ share the same concentration gradient, $\zeta = 1.0\ \mathrm{kg_S\ m^{-4}}$, and the same mean concentration, $S_0 = 0.15\ \mathrm{kg_S\ m^{-3}}$, but differ by the Reynolds number. Both simulations produce wide distributions because of small average concentration combined with a strong gradient and the specific growth rate reduction, when it takes place, is more pronounced. The influence of the Reynolds number on the specific growth rate reduction seems moderate, probably because the two Reynolds number are not sufficiently different. However, in the stationary simulation performed here, a higher Reynolds number leads to higher concentration fluctuations which means a wider distribution. The fact that the growth rate reduction increases with the Reynolds number is therefore consistent.

These results can be analyzed from an experimental point of view also. A general observation is that a specific growth rate reduction of less than a few percent is probably impossible to

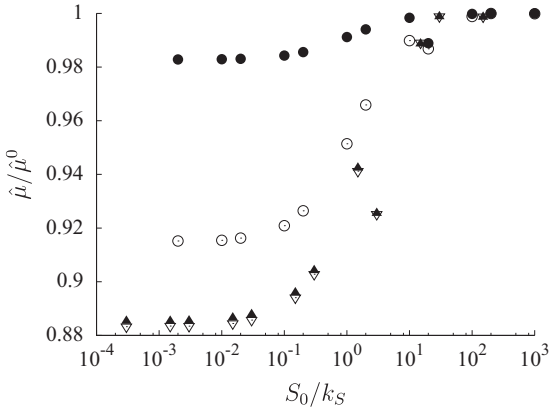

Fig. 11. Specific growth rate reduction with respect to the ratio $\langle S\rangle/k_S$ for the different simulations. ⋆: Re=68, $\zeta = 1\ \mathrm{kg_S\ m^{-4}}$, $S_0 = 0.15\ \mathrm{kg_S\ m^{-3}}$; ▿: Re=110, $\zeta = 1\ \mathrm{kg_S\ m^{-4}}$, $S_0 = 0.15\ \mathrm{kg_S\ m^{-3}}$; ●: Re=110, $\zeta = 0.1\ \mathrm{kg_S\ m^{-4}}$, $S_0 = 1.0\ \mathrm{kg_S\ m^{-3}}$; and ○: Re=110, $\zeta = 5\ \mathrm{kg_S\ m^{-4}}$, $S_0 = 1.0\ \mathrm{kg_S\ m^{-3}}$.

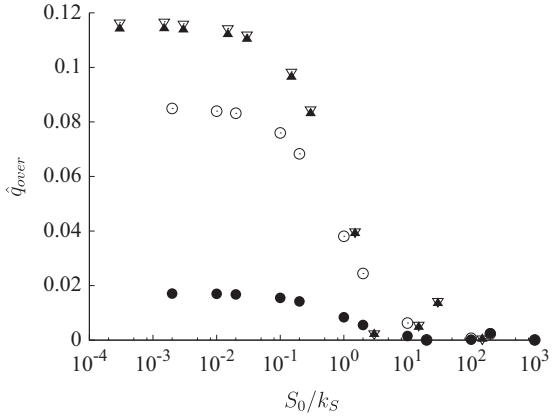

Fig. 12. Specific growth rate reduction with respect to the ratio $\langle S\rangle/k_S$ for the different simulations. ⋆: Re=68, $\zeta = 1\ \mathrm{kg_S\ m^{-4}}$, $S_0 = 0.15\ \mathrm{kg_S\ m^{-3}}$; ▿: Re=110, $\zeta = 1\ \mathrm{kg_S\ m^{-4}}$, $S_0 = 0.15\ \mathrm{kg_S\ m^{-3}}$; ●: Re=110, $\zeta = 0.1\ \mathrm{kg_S\ m^{-4}}$, $S_0 = 1.0\ \mathrm{kg_S\ m^{-3}}$; and ○: Re=110, $\zeta = 5\ \mathrm{kg_S\ m^{-4}}$, $S_0 = 1.0\ \mathrm{kg_S\ m^{-3}}$.

detect through experimental measurements. The consequences of imperfect micromixing can be appreciated following a vertical line at constant S_0/k_S starting from the top of the graph. If the mixing is intense, no growth rate reduction takes places. As the concentration heterogeneities appear a growth rate reduction and a by product formation occur but they may be undetectable experimentally. Then the effects become more pronounced and a reduction of 10% can be achieved in some cases. It is essential to note that, in practice, one would measure the same average substrate concentration but different specific growth rates (affected by the actual micromixing efficiency). In order to fit these data, with a Monod law, it would be necessary to adjust $\mu_{\max}$ or k_S or both. This is another clear evidence that from a purely physical point of view, micromixing can influence the identification of biological constants (Linkès et al., 2012).

Fig. 12 shows the rate of by-product formation with respect to $\langle S\rangle/k_S$ for the different flow configuration simulated. It can be seen that using the proposed model, some by-product is formed as soon as the mean substrate concentration becomes smaller than $10k_S$. In the region of moderate limitation $\langle S\rangle/k_S \approx 1$, overflow metabolism can represent around 5% of the total carbon flux. This may not be sufficient to be detected, in particular if this by-product can be further re-assimilated (Enfors et al., 2001), but it can explain the observed diminution of the specific growth rate and the increase of the conversion yield of substrate into biomass in imperfectly mixed bioreactors (George et al., 1998).

The main observations are that the heterogeneity of the substrate concentration field is responsible for a decrease in the apparent specific growth rate and an increase in the by-product formation. These conclusions can only be drawn through the use of a metabolic model in conjunction with the knowledge of the substrate uptake rate distribution. The two elements are equally important: it is remarkable that using a metabolic model while assuming homogeneity in the computational domain, i.e. without considering the actual distribution would lead to erroneous results: the specific growth rate would be overestimated and the amount of by-product formed underestimated. Similarly, accounting for a heterogeneous concentration field without considering a metabolic response would not produce the desired effects.

6. Conclusion

Direct numerical simulation combined with Lagrangian particle tracking and scalar field calculations in a statistically steady homogeneous and isotropic turbulence were conducted. In the present work neither the cell adaptation to the concentration fluctuations nor the modification of the concentration field due to the cell assimilation were considered. So the consequences of concentration field heterogeneities on the calculation of apparent biokinetic rates were investigated from a purely physical point of view. Through an analytic approach, the local heterogeneities seen by the individual microorganisms of a given population (characterized by the affinity constant k_S) can be integrated at the population scale in order to produce a mass flux distribution. These analytical developments were used to validate the numerical simulations. Using a metabolic model to compute the internal reaction rates and integrating over the entire population of particles (cells) reveals that substrate heterogeneities, or imperfect micromixing, lead to a reduction of the mean specific growth rate, an increase of by-products formation whereas the overall substrate consumption rate remains unchanged. In most modelling approaches of bioreactors, including CFD simulations, the assumption that distribution of the concentration is uniform in a computational mesh is generally made. The present work provides a quantification of the errors induced when the aforementioned assumption is not valid. Beyond the necessary reference to a metabolic model, the use of a subgrid model to account for the substrate concentration distribution below the resolved scale is certainly a major way for improving the reliability of a bioreactor model.

References

Amanullah, A., McFarlane, C.M., Emery, A.N., Nienow, A.W., 2001. Scale-down model to simulate spatial pH variations in large-scale bioreactors. Biotechnol. Bioeng. 73 (5), 390–399.

Baldyga, J., Bourne, J.R., 2003. Turbulent Mixing and Chemical Reactions. John Wiley and Sons, Chichester.

Boivin, M., Simonin, O., Squires, K., 1998. Direct numerical simulation of turbulence modulation by particles in isotropic turbulence. J. Fluid Mech. 375 (1), 235–263.

Bourne, J.R., 2003. Mixing and the selectivity of chemical reactions. Org. Process Res. Dev. 7 (4), 471–508.

Bylund, F., Collet, E., Enfors, S.-O., Larsson, G., 1998. Substrate gradient formation in the large-scale bioreactor lowers cell yield and increases by-product formation. Bioprocess Biosyst. Eng. 18, 171–180.

Chassagnole, C., Noisommit-Rizzi, N., Schmid, J.W., Mauch, K., Reuss, M., 2002. Dynamic modeling of the central carbon metabolism of Escherichia coli. Biotechnol. Bioeng. 79 (1), 53–73.

Couzinet, A., Bédat, B., Simonin, O., 2008. Numerical study and lagrangian modelling of turbulent heat transport. Flow Turbul. Combust. 80 (1), 37–46.

Delafosse, A., 2008. Analyse et étude Numérique des Effets de Mélange dans un Bioréacteur. (Ph.D. Thesis), Institut National des Sciences Appliquées, Toulouse, France.

Delafosse, A., Morchain, J., Guiraud, P., Liné, A., 2009. Trailing vortices generated by a rushton turbine: assessment of RANS and large eddy simulations. Chem. Eng. Res. Des. 87 (4), 401–411.

Delvigne, F., Boxus, M., Ingels, S., Thonart, P., et al., 2009. Bioreactor mixing efficiency modulates the activity of a prpoS:: GFP reporter gene in *E. coli*. Microb. Cell Fact. 8 (1), 15.

Dunlop, E., Ye, S., 1990. Micromixing in fermentors: metabolic changes in *Saccharomyces cerevisiae* and their relationship to fluid turbulence, pp. 854–864. In: Garcia, J., Cha, H., Rao, G., Marten, M., Bentley, W. (Eds.), 2009. Microbial nar-GFP cell sensors reveal oxygen limitations in highly agitated and aerated laboratory-scale fermentors. Microb. Cell Fact. 8 (1), 6.

Enfors, S.O., Jahic, M., Rozkov, A., Xu, B., Hecker, M., Jürgen, B., Krüger, E., Schweder, T., Hamer, G., O'Beirne, D., Noisommit-Rizzi, N., Reuss, M., Boone, L., Hewitt, C., McFarlane, C., Nienow, A., Kovacs, T., Trägårdh, C., Fuchs, L., Revstedt, J., Friberg, P.C., Hjertager, B., Blomsten, G., Skogman, H., Hjort, S., Hoeks, F., Lin, H.Y., Neubauer, P., van der Lans, R., Luyben, K., Vrabel, P., Manelius, A., 2001. Physiological responses to mixing in large scale bioreactors. J. Biotechnol. 85 (2), 175–185.

Eswaran, V., Pope, S., 1988. An examination of forcing in direct numerical simulations of turbulence. Comput. Fluids 16, 257–278.

Ferenci, T., 1996. Adaptation to life at micromolar nutrient levels: the regulation of *Escherichia coli* glucose transport by endoinduction and camp. FEMS Microbiol. Rev. 18 (4), 301–317.

Garcia, J., Cha, H., Rao, G., Marten, M., Bentley, W., 2009. Microbial nar-GFP cell sensors reveal oxygen limitations in highly agitated and aerated laboratory-scale fermentors. Microb. Cell Fact. 8 (1), 6.

George, S., Larsson, G., Olsson, K., Enfors, S.-O., 1998. Comparison of the baker's yeast process performance in laboratory and production scale. Bioprocess Biosyst. Eng. 18, 135–142.

Hansford, G., 1966. The effect of equipment scale and degree of mixing on continuous fermentation yield at low dilution rates, pp. 85–96. In: Garcia, J., Cha, H., Rao, G., Marten, M., Bentley, W. (Eds.), 2009. Microbial nar-GFP cell sensors reveal oxygen limitations in highly agitated and aerated laboratory-scale fermentors. Microb. Cell Fact. 8 (1), 6.

Hewitt, C.J., Nebe-Von Caron, G., Axelsson, B., McFarlane, C.M., Nienow, A.W., 2000. Studies related to the scale-up of high-cell-density *E. coli* fed-batch fermentations using multiparameter flow cytometry: effect of a changing microenvironment with respect to glucose and dissolved oxygen concentration. Biotechnol. Bioeng. 70 (4), 381–390.

KaSZ, F., Junne, S., Neubauer, P., Wiechert, W., Oldiges, M., 2014. Process inhomogeneity leads to rapid side product turnover in cultivation of *Corynebacterium glutamicum*. Microb. Cell Fact. 13 (1), 6, URL ⟨http://www.microbialcellfactories.com/content/13/1/6⟩.

Koch, A.L., Wang, H.C., 1982. How close to the theoretical diffusion limit do bacterial uptake systems function? Arch. Microbiol. 131 (1), 36–42.

Lapin, A., Muller, D., Reuss, M., 2004. Dynamic behavior of microbial populations in stirred bioreactors simulated with euler-lagrange methods: traveling along the lifelines of single cells. Ind. Eng. Chem. Res. 43 (16), 4647–4656.

Lapin, A., Schmid, J., Reuss, M., 2006. Modeling the dynamics of *E. coli* populations in the three-dimensional turbulent field of a stirred-tank bioreactor – a structured – segregated approach. Chem. Eng. Sci. 61 (14), 4783–4797.

Larsson, G., Tornkvist, M., Wernersson, E., Trägårdh, C., Noorman, H., Enfors, S., 1996. Substrate gradients in bioreactors: origin and consequences. Bioprocess Biosyst. Eng. 14 (6), 281–289.

Lin, H.Y., Mathiszik, B., Xu, B., Enfors, S.-O., Neubauer, P., 2001. Determination of the maximum specific uptake capacities for glucose and oxygen in glucose-limited fed-batch cultivations of *Escherichia coli*. Biotechnol. Bioeng. 73 (5), 347–357.

Linkès, M., Martins Afonso, M., Fede, P., Morchain, J., Schmitz, P., 2012. Numerical study of substrate assimilation by a microorganism exposed to fluctuating concentration. Chem. Eng. Sci. 81 (0), 8–19.

Morchain, J., Gabelle, J.-C., Cockx, A., 2014. A coupled population balance model and CFD approach for the simulation of mixing issues in lab-scale and industrial bioreactors. AIChE J. 60 (1), 27–40, URL ⟨http://dx.doi.org/10.1002/aic.14238⟩.

Natarajan, A., Srienc, F., 1999. Dynamics of glucose uptake by single *Escherichia coli* cells. Metab. Eng. 1 (4), 320–333.

Natarajan, A., Srienc, F., 2000. Glucose uptake rates of single *E. coli* cells grown in glucose-limited chemostat cultures. J. Microbiol. Methods 42 (1), 87–96.

Oosterhuis, N.M.G., Kossen, N.W.F., 1984. Dissolved oxygen concentration profiles in a production-scale bioreactor. Biotechnol. Bioeng. 26 (5), 546–550.

Pandya, R., Mashayek, F., 2003. Non-isothermal dispersed phase of particles in turbulent flow. J. Fluid Mech. 475 (1), 205–245.

Reade, W., Collins, L., 2000. Effect of preferential concentration on turbulent collision rates. Phys. Fluids 12, 2530.

Taulbee, D.B., Mashayek, F., Barré, C., 1999. Simulation and Reynolds stress modeling of particle-laden turbulent shear flows. Int. J. Heat Fluid Flow 20 (4), 368–373.

Taylor, J.R., Stocker, R., 2012. Trade-offs of chemotactic foraging in turbulent water. Science 338 (6107), 675–679.

Vràbel, P., van der Lans, R.G., van der Schot, F.N., Luyben, K.C., Xu, B., Enfors, S.-O., 2001. CMA: integration of fluid dynamics and microbial kinetics in modelling of large-scale fermentations. Chem. Eng. J. 84 (3), 463–474.

Xu, B., Jahic, M., Enfors, S.-O., 1999. Modeling of overflow metabolism in batch and fed-batch cultures of *Escherichia coli*. Biotechnol. Prog. 15 (1), 81–90.

Yeung, P., 1998. Correlations and conditional statistics in differential diffusion: scalars with uniform mean gradients. Phys. Fluids 10, 2621.